PHYSICAL REVIEW

LETTERS

Wavelet Transform of Multifractals

A. Arneodo and G. Grasseau

Centre de Recherche Paul Pascal, Domaine Universitaire, 33405 Talence CEDEX, France

M. Holschneider

*Centre de Physique Théorique, Centre National de la Recherche Scientifique Luminy,
13288 Marseille CEDEX, France*

(Received 11 January 1988)

We present the wavelet transform as a mathematical microscope which is well suited for studying the local scaling properties of fractal objects. We apply this technique to probability measures on self-similar Cantor sets and to the golden-mean trajectories on two-tori at the onset of chaos.

Most previous characterizations of multifractals[1,2] have brought a global description of the scaling properties through the determination of the continuous spectrum of scaling indices α and their densities $f(\alpha)$. Although the $f(\alpha)$ spectrum is closely related to the generalized fractal dimensions[3] D_q, it is unfortunately powerless to describe the spatial locations of these singularities. An analogous situation is faced in signal analysis, where power spectra extracted from recorded time series suffer from a similar deficiency. The power spectrum identifies the underlying frequencies and quantifies their relative contributions, but says nothing about their temporal locations. In recent analysis[4] of seismic data and acoustic signals, the Fourier transform has been supplanted by a transformation which gives a representation of the signal as a function of both time and frequency: the wavelet transform.[5] The purpose of this Letter is to introduce the wavelet transform as a natural tool for investigating the self-similar properties of fractal objects at different length scales.[6]

The wavelet transform consists of expanding functions over wavelets which are constructed from a single function g by means of dilations and translations.[5] Let us consider a fractal represented by a real function f; let g be a regular complex-valued function that is localized around zero and some of whose moments are zero [g should be at least of zero mean: $\int g(x)dx = 0$]. Then the wavelet transform of f with respect to the wavelet g

is defined as

$$T(a,b) = \frac{1}{a}\int \bar{g}\left(\frac{x-b}{a}\right)f(x)dx, \quad a>0, b \in \mathcal{R}. \quad (1)$$

This transformation can be seen as a mathematical microscope whose position and magnification are b and $1/a$, respectively, and whose optics are given by the choice of the specific wavelet g. No information about f is lost since this transformation is invertible for a large class of functions[5] f. For a fractal measure $dm(x)$, we define its transform as

$$T(a,b) = \frac{1}{a^n}\int \bar{g}\left(\frac{x-b}{a}\right)dm(x), \quad a>0, b \in \mathcal{R}, \quad (2)$$

where the normalization factor $1/a^n$ may be chosen to best reveal the scaling structure of the fractal measure under consideration.

Scalings and wavelets.— A typical property of fractals is that they are asymptotically self-similar at small length scales. Thus, looking near an arbitrary point x_0 at different scales, we always find the same function up to a scaling factor. Defining $f_{x_0}(x) = f(x_0+x) - f(x_0)$, then we have

$$f_{x_0}(\lambda x) \sim \lambda^{a(x_0)} f_{x_0}(x). \quad (3)$$

For a wavelet which decays sufficiently fast at infinity, this scaling behavior of f is mirrored by the wavelet

transform which scales like[6]

$$T(\lambda a, x_0 + \lambda b) = \lambda^{a(x_0)} T(a, x_0 + b),\qquad (4)$$

i.e., with the same exponent $a(x_0)$ as f. Therefore, every local singularity of f produces a conelike structure in the wavelet transform pointing towards the point $(a = 0,$ $b = x_0)$ at the border of the half-plane where this singularity of type a is located.[5,6] A fairly general theoretical result is that a high regularity of the function is reflected in the wavelet transform by a rapid decay of the coefficients $T(a,b)$ in the limit $a \to 0^+$. A straightforward integration shows that the local scaling exponent $a(x_0)$ of $dm(x)$ turns into an exponent $\hat{a}(x_0)$ $= a(x_0) - n$ in the wavelet transform, where n is the normalization exponent in Eq. (2).

Usually, relation (3) will not hold for all $\lambda \in \mathcal{R}$ but rather for an infinite sequence $\lambda_m \sim \beta^m$, $m \in \mathbb{Z}$. Henceforth, the exponent a is complex and the fractal shows oscillatory scaling behavior. In the wavelet transform, oscillations of period $\ln\beta$ exist around a straight line with slope a when $\ln|T(a,x_0)|$ is plotted versus $\ln a$. Similar periodic oscillations have been found in the log-log plot measurement of the Renyi dimensions of highly self-similar Cantor sets.[7]

In this Letter we use a real wavelet g of Gaussian type: $g(x) = (1 - x^2)\exp(-x^2/2)$ to investigate some fractal invariant measures of well-known dynamical systems. We choose the rescaling exponent in Eq. (2) equal to $n = 2$, such that in all examples we shall consider, the local singularities will correspond to a power-law divergence of the wavelet transform T in the limit $a \to 0^+$ $(\hat{a} < 0)$.

Probability measures on Cantor sets.— A simple example is the standard triadic Cantor set. We initially divide the unit interval $[0,1]$ in two intervals each of length $l = l_1 = l_2 = \frac{1}{3}$. These intervals receive, respectively, the probability p_1 and p_2 with $p_1 \geq p_2$. At the next stage of the construction of the measure, this same process is repeated on each of these two subintervals. The spectrum of singularities of this measure can be understood with use of the technique of "kneading sequence."[1] Any point of the Cantor set can be addressed by an infinite sequence of symbols L and R where L (left) labels the interval with maximal probability p_1 and R (right) labels the interval with minimal probability p_2. Clearly, the sequence $LLLL \ldots$ is associated with the singularity $a_{min} = -\ln p_1/\ln 3$, while the sequence $RRRR \ldots$ is associated with the singularity a_{max} $= -\ln p_2/\ln 3$. Other more complicated kneading sequences yield a values which range between a_{min} and a_{max}.

In Fig. 1(a), we show an overview of the wavelet transform of the uniform triadic Cantor set with $p_1 = p_2 = \frac{1}{2}$. The successive pitchfork branchings observed when increasing the magnification $(1/a)$ provide an instructive illustration of the construction process of
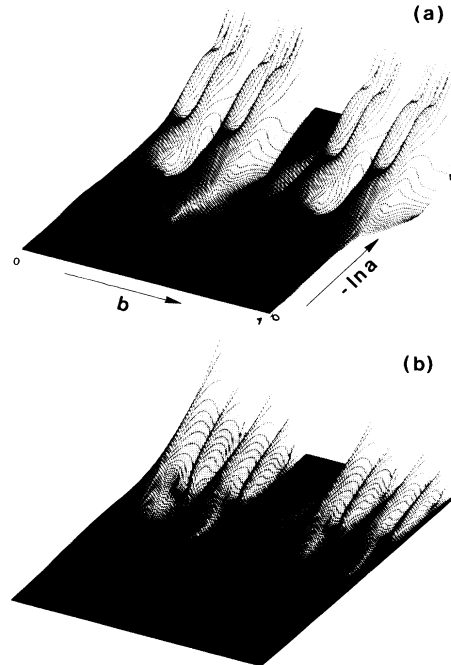

FIG. 1. The wavelet transform $[\mathrm{sgn}(T) |T(a,b)|^{1/2}]$ of the triadic Cantor set with (a) uniform measure $p_1 = p_2 = \frac{1}{2}$, and (b) two distinct measures $p_1 = \frac{3}{4}$, $p_2 = \frac{1}{4}$; the scales in (a) and (b) are different and $n = 2$ in Eq. (2).

the Cantor set. The positions of the local singularities of the measure are easily identified as spatial points b^* where the wavelet transform displays an oscillatory (with period $P = \ln 3$) power-law divergence. Each of these points is a point of the Cantor set. At each of these points, the power-law exponent is $\hat{a}(b^*) = \ln 2/\ln 3 - 2$, which corroborates the theoretical prediction[1] that all the singularities have the same strength $a = \ln 2/\ln 3$ with the density $f = \ln 2/\ln 3$. The Legendre transform of this spectrum confirms that the uniform Cantor set is self-similar with dimensions $D_q = \ln 2/\ln 3$, for all q.

In Fig. 1(b), we show the wavelet transform of the fractal measure generated with $p_1 = \frac{3}{4}$ and $p_2 = \frac{1}{4}$. Although the support of the measure is the same geometrical object as in Fig. 1(a), a simple visual inspection of the wavelet transform allows us to differentiate the nonuniform from the uniform Cantor set. While the power-law divergence of T still clearly indicates the location of the singularities at the points of the Cantor set, the power-law exponent is obviously no longer unique and is actually found to range between $\hat{a}_{min}$ $= -\ln p_1/\ln 3 - 2$ $(b = 0)$ to $\hat{a}_{max} = -\ln p_2/\ln 3 - 2$ $(b = 1)$. Again this numerical result confirms the theoretical predictions[1] of the existence of a finite range of scaling indices $a \in [a_{min}, a_{max}]$, with additional information concerning the spatial location of each singularity. In Fig. 2, we have cut the half-plane along $b = b^*$, where b^* is the point which corresponds to the kneading sequence $RRRRRRRLLLL \ldots LLL \ldots$; when plotting
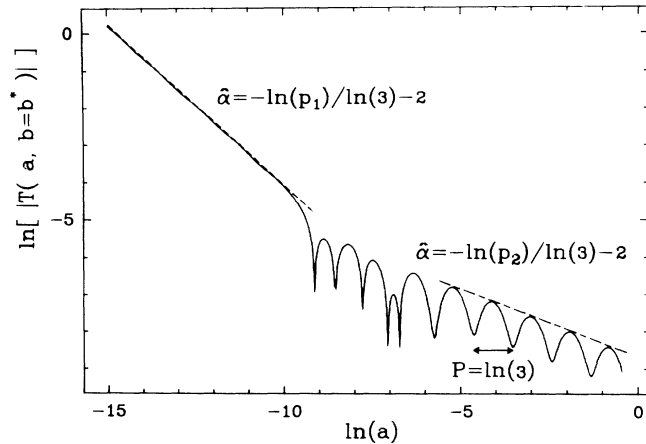
FIG. 2. $\ln|T(a,b=b^*)|$ (arbitrary scale) vs $\ln a$ for the nonuniform Cantor set where b^* corresponds to the kneading sequence $RRRRRRRRLLLL \ldots LLL \ldots$.

$\ln|T(a,b^*)|$ vs $\ln a$ we find a value of $\hat{a} \in [\hat{a}_{min}, \hat{a}_{max}]$. Indeed, a crossover effect is observed from the exponent $\hat{a}_{max}$ at large scale to the exponent $\hat{a}_{min}$ at smaller scale because of the tail of L's. We note that the period of oscillations is again $P = \ln 3 = \ln l^{-1}$ which attests that, up to a scaling factor, the fractal measure is invariant under dilation of the length scale by a factor $\beta = l^{-1} = 3$ in the neighborhood of b^*.

Quasiperiodic trajectories at the onset of chaos.— The transition from quasiperiodicity to chaos is commonly modeled by circle maps such as the sine map[8]

$$\theta_{i+1} = f_{K,\Omega}(\theta_i) = \theta_i + \Omega - K/2\pi \sin(2\pi\theta_i). \quad (5)$$

Recently, a numerical investigation[1] of the critical sine map for $K = 1$ has revealed the universal properties of the spectrum of singularities $f(\alpha)$ of the golden-mean trajectory with winding number $W = W^* = (\sqrt{5} - 1)/2$. The associated invariant measure develops a whole spectrum of singularities with scaling indices in a finite range $0.6326 \ldots \leq \alpha \leq 1.8980 \ldots$ giving rise to nontrivial dimensions D_q and spectrum $f(\alpha)$.

Figure 3(a) shows the wavelet transform of the golden-mean trajectory which displays structure at all scales. The a dependence of $T(a,0)$ yields the exponent $\hat{a}_{max} = \alpha_{max} - 2$, where $\alpha_{max} = \ln W^*/\ln \alpha_{gm}^{-1}$ matches the renormalization-group predictions[1,8] based on Shenker's remark that the distances around $\theta = 0$ scale down by a universal factor $\alpha_{gm} = 1.2885 \ldots$ when the trajectory is truncated at two consecutive Fibonacci numbers F_n, F_{n+1}. This local self-similarity shows up through small amplitude periodic oscillations around this slope with period $P = \ln \alpha_{gm}$. In Fig. 4, we have performed the same analysis at $b = \Omega^*(K = 1)$ [$\Omega^*(K)$ is such that $W = W^*$], i.e., at the first image of zero. The slope is now $\hat{a}_{min} = \alpha_{min} - 2$ where $\alpha_{min} = \ln W^*/\ln \alpha_{gm}^{-3}$ is the local exponent. This can be deduced directly from α_{max} because of the cubic nature of the inflection point of
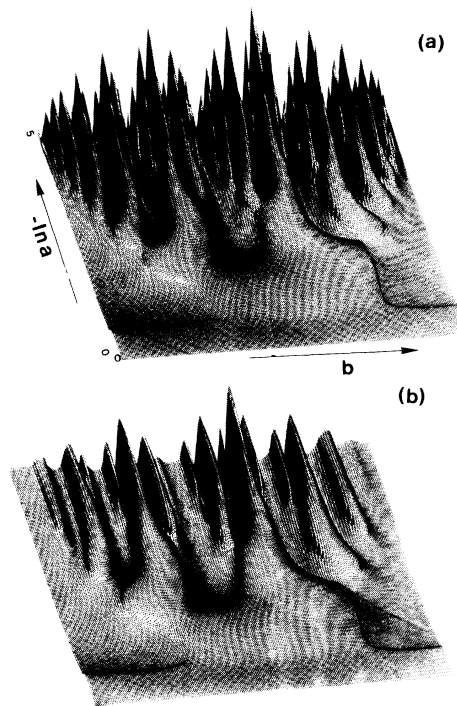

FIG. 3. The wavelet transform $[sgn(T)|T(a,b)|^{1/2}]$ of the golden-mean trajectory calculated with the sine map (5) for (a) $K = 1$ and (b) $K = 0.9$ [$n = 2$ in Eq. (2)].

$f_{K=1,\Omega^*}$ at zero.[1] In the inset of Fig. 4, the slope has been subtracted to reveal the oscillations of period $P = \ln \alpha_{gm}^3$ which reflect the scaling properties in the neighborhood of every iterate of zero. In Fig. 5, the wavelet transform of the critical golden-mean trajectory is shown in a two-color representation: The black re-
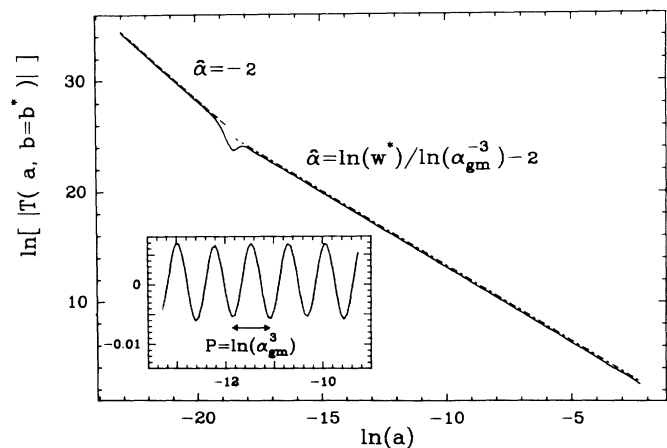

FIG. 4. The wavelet transform $\ln|T(a,b=b^*)|$ vs $\ln a$ of the critical golden-mean trajectory calculated with the sine map (5) for $\Omega = \Omega^*$, $K = 1$, and $b^* = f_{K=1,\Omega^*}(0) = \Omega^*$. The golden-mean trajectory has been approximated by the super-stable W_{25} cycle ($W_n = F_n/F_{n+1}$) which explains the trivial slope $\hat{a} = -n = -2$ observed at small scales.
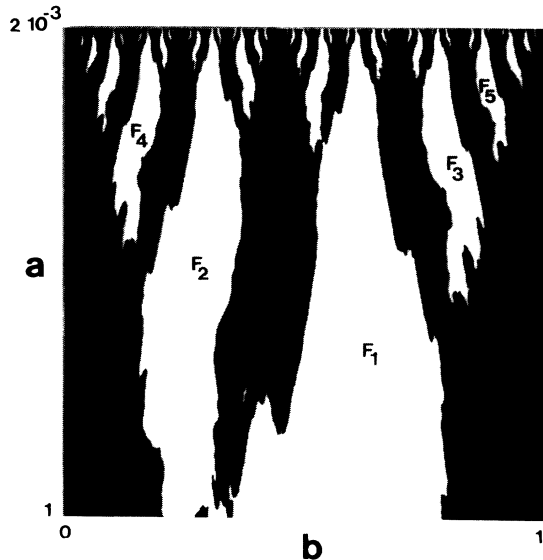
FIG. 5. The wavelet transform of the critical golden-mean trajectory calculated with the sine map (5) for $K=1$. The black $(T < \tilde{T})$ and white $(T \geq \tilde{T})$ coding is obtained when defining on each $a=$constant line a threshold $\tilde{T} = \delta \max T(a,b)$ $(\delta > 0)$.

gions correspond to $T < \tilde{T}$, where the threshold $\tilde{T}$ is defined in proportion to $\max T(a,b)$ (>0) on each $a =$ constant line in such a way that the white cones point to the dominant singularities situated at the images of zero. The most prominent cones define the F_n iterates of zero; they actually accumulate at zero in an alternating geometric progression governed by the exponent α_{gm}. Each one of these white cones is itself an accumulation limit of white cones (the F_m iterates of the F_n iterates of zero) but with a different convergence rate α_{gm}^3 because of the cubic inflection point. This hierarchy of white cones continues at smaller and smaller scales; it is at the heart of the renormalization-group analysis of this transition to chaos.[8] We mention that when defining the threshold $\tilde{T}$ with respect to $\min T(a,b)$ (<0), one can identify in the same way the weakest singularities located at zero and its inverse images. Then the main white cones corresponding to the F_n inverse images of zero will converge in an alternating geometric way to zero at rate α_{gm}, while secondary white cones will accumulate to the main white cones at the same rate α_{gm} and so on.

For $K < 1$, the sine map $f_{K, \Omega^*(K)}$ is a diffeomorphism which is analytically conjugate to a pure rotation.[8] The generalized fractal dimensions are invariant under a smooth coordinate change; this implies that $D_q = 1$. Indeed, the invariant measure has no singularities and so the scaling is trivial with a single index $\alpha = 1$. In Fig. 3(b), we show the wavelet transform computed for

$K = 0.9$; the large scale behavior is mostly unaffected by this deviation from criticality. The structures which emerge at large scales are progressively smoothed out at small scales and $|T(a,b)|$ unescapably decreases to zero in the limit $a \to 0^+$. Henceforth, the complex hierarchy of white cones observed at criticality in Fig. 5 disappears at small scales. This loss of structure occurs at larger and larger scales as K is decreased, i.e., as the departure from criticality is increased. This crossover behavior[9] from an invariant measure which retains memory of its critical properties at large scales, to a nonsingular invariant measure at small scales is analogous to crossover effects observed in phase transition phenomena near to critical points. It can be understood with use of a renormalization-group approach as a crossover from a strong-coupling $(K=1)$ to a weak-coupling $(K=0)$ fixed point.[9]

In summary, we have pointed out that the wavelet transform is able to capture the full complexity of the self-similar properties of multifractals. Since its implementation on a computer is not excessively time consuming and does not require enormous storage, the wavelet transform provides a very efficient tool for analyzing fractal objects. Its application to a variety of physical situations, such as percolation, growth phenomena, and fully developed turbulence, looks very promising.

[1]T. C. Halsey, M. H. Jensen, L. P. Kadanoff, I. Procaccia, and B. I. Shraiman, Phys. Rev. A 33, 1141 (1986).

[2]P. Collet, J. L. Lebowitz, and A. Porzio, J. Stat. Phys. 47, 609 (1987).

[3]P. Grassberger and I. Procaccia, Physica (Amsterdam) 3D, 34 (1984).

[4]P. Goupillaud, A. Grossmann, and J. Morlet, Geoexploration 23, 85 (1984); R. Kronland-Martinet, J. Morlet, and A. Grossmann, Int. J. Pattern Recognit. Artif. Intelligence, Special Issue on Expert Systems and Pattern Analysis (1987).

[5]A. Grossmann and J. Morlet, in Mathematics and Physics, Letures on Recent Results, edited by L. Streit (World Scientific, Singapore, 1987); I. Daubechies and T. Paul, in Proceedings of the Eighth Congress of Mathematical Physics, Marseille, France, 1986, edited by R. Seneor and M. Mebkhout (World Scientific, Singapore 1987); P. G. Lemarie and Y. Meyer, Rev. Iberoam. 1, 1286 (1987).

[6]M. Holschneider, J. Stat. Phys. 50, 963 (1988).

[7]R. Badii and A. Politi, Phys. Lett. 104A, 303 (1984); L. A. Smith, J. D. Fournier, and E. A. Spiegel, Phys. Lett. 114A, 465 (1986).

[8]S. J. Shenker, Physica (Amsterdam) 5D, 405 (1982); M. J. Feigenbaum, L. P. Kadanoff, and S. J. Shenker, Physica (Amsterdam) 5D, 370 (1982); S. Ostlund, D. Rand, J. P. Sethna, and E. D. Siggia, Physica (Amsterdam) 8D, 303 (1983).

[9]A. Arneodo and M. Holschneider, Phys. Rev. Lett. 58, 2007 (1987).

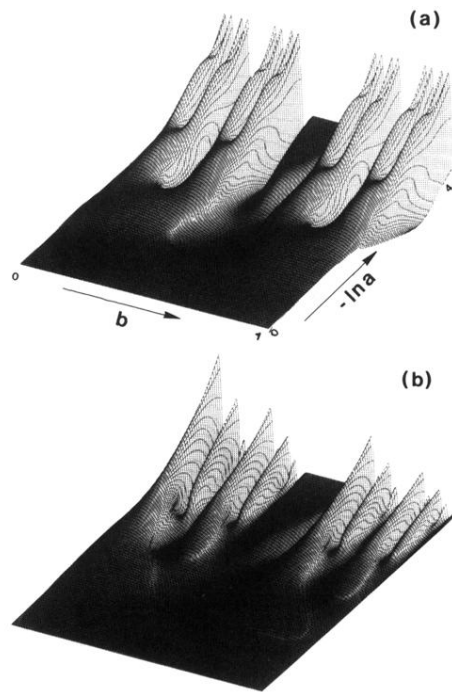FIG. 1. The wavelet transform $[\mathrm{sgn}(T)\,|\,T(a,b)\,|^{1/2}]$ of the triadic Cantor set with (a) uniform measure $p_1 = p_2 = \frac{1}{2}$, and (b) two distinct measures $p_1 = \frac{3}{4}$, $p_2 = \frac{1}{4}$; the scales in (a) and (b) are different and $n = 2$ in Eq. (2).
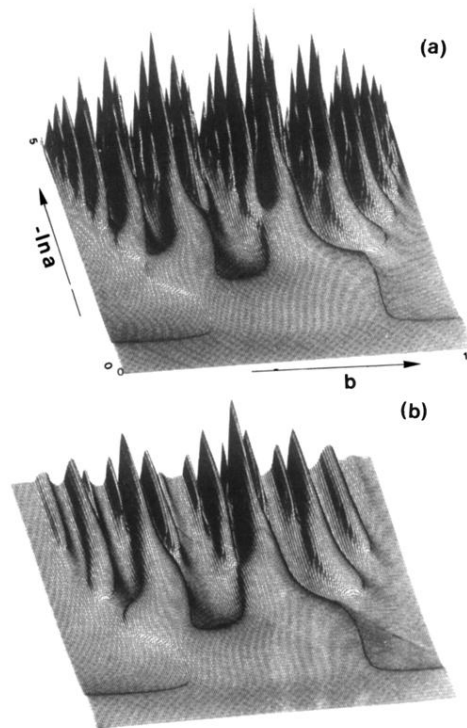
FIG. 3. The wavelet transform $[\mathrm{sgn}(T) \, | \, T(a,b) \, |^{1/2}]$ of the golden-mean trajectory calculated with the sine map (5) for (a) $K=1$ and (b) $K=0.9$ [$n=2$ in Eq. (2)].
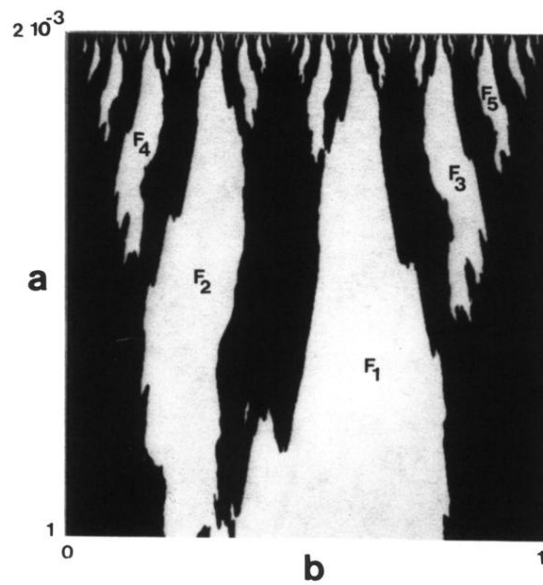
FIG. 5. The wavelet transform of the critical golden-mean trajectory calculated with the sine map (5) for $K = 1$. The black $(T < \tilde{T})$ and white $(T \geq \tilde{T})$ coding is obtained when defining on each a=constant line a threshold $\tilde{T} = \delta \max T(a, b)$ $(\delta > 0)$.